

# Ly $\alpha$ excess in high redshift radio galaxies: a signature of star formation.\*

M. Villar-Martín<sup>1</sup>, A. Humphrey<sup>2</sup>, C. De Breuck<sup>3</sup>, R. Fosbury<sup>4</sup>, L. Binette<sup>2</sup>, J. Vernet<sup>3</sup>

<sup>1</sup>*Instituto de Astrofísica de Andalucía (CSIC), Aptdo. 3004, 18080 Granada, Spain*

<sup>2</sup>*Instituto de Astronomía, UNAM, Ap. 70-264, 04510, DF, México*

<sup>3</sup>*European Southern Observatory, Karl Schwarzschild Str. 2, D-85748 Garching bei München, Germany*

<sup>4</sup>*ST-ECF, Karl Schwarzschild Str. 2, D-85748 Garching bei München, Germany*

## ABSTRACT

About 54% of radio galaxies at  $z \geq 3$  and 8% of radio galaxies at  $2 \lesssim z < 3$  show unusually strong Ly $\alpha$  emission, compared with the general population of high redshift ( $z \gtrsim 2$ ) radio galaxies. These Ly $\alpha$ -excess objects (LAEs) show Ly $\alpha$ /HeII values consistent with or *above* standard photoionization model predictions.

We reject with confidence several scenarios to explain the unusual strength of Ly $\alpha$  in these objects: shocks, low nebular metallicities, high gas densities and absorption/scattering effects. We show that the most successful explanation is the presence of a young stellar population which provides the extra supply of ionizing photons required to explain the Ly $\alpha$  excess in at least the most extreme LAEs (probably in all of them). This interpretation is strongly supported by the tentative trend found by other authors for  $z \geq 3$  radio galaxies to show lower UV-rest frame polarization levels, or the dramatic increase on the detection rate at submm wavelengths of  $z > 2.5$  radio galaxies. The enhanced star formation activity in LAEs could be a consequence of a recent merger which has triggered both the star formation and the AGN/radio activities.

The measurement of unusually high Ly $\alpha$  ratios in the extended gas of some high redshift radio galaxies suggests that star formation activity occurs in spatial scales of tens of kpc.

We argue that, although the fraction of LAEs may be incompletely determined, both at  $2 \lesssim z < 3$  and at  $z \geq 3$ , the much larger fraction of LAEs found at  $z \geq 3$  is a genuine redshift evolution and not due to selection effects. Therefore, our results suggest that the radio galaxy phenomenon is more often associated with a massive starburst at  $z > 3$  than at  $z < 3$ .

**Key words:** cosmology: observations, early Universe; galaxies: active; galaxies: evolution

## 1 INTRODUCTION

High redshift powerful radio galaxies (HzRG,  $z \gtrsim 2$ ) are characterized by an emission line spectrum which is rich in emission lines of different ionization species. In the optical (UV rest frame), Ly $\alpha$  is usually the strongest emission line, followed by CIV $\lambda$ 1550, HeII $\lambda$ 1640, CIII] $\lambda$ 1909 and, less frequently, NV $\lambda$ 1240 (CIV, HeII, CIII] and NV hereafter).

De Breuck et al. (2000a, DB00a hereafter) observed that Ly $\alpha$  is unusually strong in some HzRG, most of which are at  $z \gtrsim 3$ . They also found that the Ly $\alpha$  equivalent width increases at  $z \gtrsim 3$  and the ratios of Ly $\alpha$  to CIV, CIII] and HeII are roughly twice the value found for lower redshift objects ( $2 \lesssim z < 3$ ). The authors interpret these results as spectroscopic evidence for the youth of radio galaxies at  $z \gtrsim 3$ , which are still surrounded by large halos of primordial hydrogen from which the galaxy is formed.

In this paper we present a more thorough study of DB00a results. We start by quantifying (§3) the variation of the Ly $\alpha$ /HeII and Ly $\alpha$ /CIV ratios and Ly $\alpha$  luminosity with redshift for radio galaxies at  $1.8 \leq z \leq 4.4$  and inter-

\* Unpublished results are presented in this paper for the radio galaxy 1338-1941, based on observations carried out at the European Southern Observatory, Paranal (Chile) for the ESO project 69.B-0078(B).

pret the results in the light of appropriate photoionization models (described in §3) and/or scenarios (§5). The results and the cosmological consequences will be discussed in §6. Summary and conclusions will be presented in §7.

A  $\Omega_\Lambda = 0.73$ ,  $\Omega_m = 0.27$  and  $H_0 = 71 \text{ km s}^{-1} \text{ Mpc}^{-1}$  cosmology is adopted in this paper.

## 2 OBJECT SAMPLE.

The object sample has been extracted from the data set of DB00a and De Breuck et al. (2001, DB01 hereafter), which includes the largest compilation of line fluxes for  $z \gtrsim 2$  radio galaxies available. We will not consider lower  $z$  objects, for which  $\text{Ly}\alpha$  is not observable. Our final sample consists of 13 radio galaxies at  $z \gtrsim 3$  and 48 radio galaxies at  $1.8 \leq z < 3$ .

Table 1 shows the sample with some relevant information.

The original data set of De Breuck et al. includes radio galaxies from nine samples designed to find HzRG. As the authors explain, the surveys can be divided into two types (see DB00a for all appropriate references of each survey): (i) several large flux density-limited surveys such as the 3CR, MRC, BRL sample, and 6C, 7C and 8C surveys; (ii) several “filtered” surveys, which were designed to find the highest redshift objects. In the latter case, the radio spectral index flux is most often used (ultra steep spectrum sources), sometimes in combination with an angular size upper limit. Alternatively, the filter consists of a flux density interval centered around the peak in the source counts around 1 Jy.

The total sample contains 176 radio galaxies with  $z$  in the range 0.05 to 5.2. It contains a similar number of sources at  $z < 2$  and at  $z > 2$ . For the present study, we have eliminated  $\sim 110$  objects for the following reasons:

- 4 broad emission line objects ( $\text{FWHM} \gtrsim 4000 \text{ km s}^{-1}$  and/or additional quasar-like properties). These are 2313+4053 ( $z = 2.99$ , DB01), 0744+464 ( $z = 2.93$ , McCarthy 1991), 2025-218 ( $z = 2.63$ , Villar-Martín et al. 1999, Larkin et al. 2000) and 0349-211 ( $z = 2.33$ , McCarthy et al. 1991). For these objects, the UV lines have a contribution from the broad line region, where the physics is complex and not interesting for the current study.

- 2 objects with broad absorption line systems: 1908+722 ( $z = 3.53$ ) and 1115+5016 ( $z = 2.54$ ) (DB01).

- 91 objects with no  $\text{Ly}\alpha$  measurement. Except for 3 objects for which the reason is not known, in all other cases  $\text{Ly}\alpha$  is outside the observed spectral range.

- 23 objects with no measurement of CIV and HeII. The reasons are varied: for 7 objects, the CIV and HeII lines were outside the useful spectral range, or only  $\text{Ly}\alpha$  narrow band imaging fluxes are available. For 6 objects, the lines are reported to be detected, but no fluxes are provided, except for  $\text{Ly}\alpha$ . For 7 objects, the lines were within the observed spectral range, but not detected. In 2 cases HeII was outside the observed spectral range and CIV was inside, but not detected. For 1 object, the reason for the non-availability of the CIV and HeII fluxes is unknown.

Using DB01 original spectra, we have been able to measure useful upper limits (in some cases the spectra are too noisy or severely affected by sky residuals) for the CIV and/or HeII lines of several of these objects. The lower limits for the  $\text{Ly}\alpha$  ratios are shown in Table 1.

There are 10 objects with no measurement of CIV (2) or HeII (8). In all cases, except one, both lines were within the observed spectral range, but not detected. Upper limits could be measured for two objects using the original DB01 spectra. The lower limits for the  $\text{Ly}\alpha$  ratios are given in Table 1.

The following objects were part of De Breuck et al. sample, but the line fluxes of one or more of the lines of interest to us were not provided. For this reason, we present measurements based on our own long slit Keck LRISp spectroscopic data or results published by other authors.

- 4C40.36 at  $z = 2.27$  (nuclear aperture, Humphrey 2005, Humphrey et al. 2006, in prep; Vernet et al. 2001)
- 4C48.48 at  $z = 2.34$  (nuclear aperture, Humphrey 2005, Humphrey et al. 2006, in prep; Vernet et al. 2001)
- 0731+438 at  $z = 2.43$  (nuclear aperture, Humphrey 2005, Humphrey et al. 2006, in prep; Vernet et al. 2001)
- 0902+34 at  $z = 3.40$  (Martín-Mirones et al. 1995)
- 1243+036 at  $z = 3.56$  (nuclear aperture, Humphrey 2005, Humphrey et al. 2006, in prep; Vernet et al. 2001)
- 4C41.17 at  $z = 3.79$  (Dey et al. 1997)
- 1338-1941 at  $z = 4.11$  (De Breuck et al. in prep. ESO project 69.B-0078(B).)

More accurate line measurements than De Breuck et al. original data were used for:

- 2334+1545 at  $z = 2.48$ . HeII is not detected in this object. Because of the unusually narrow CIV line ( $< 500 \text{ km s}^{-1}$ ) measured by DB01 compared with  $\text{Ly}\alpha$  ( $1900 \text{ km s}^{-1}$ ) and CIII] ( $1600 \text{ km s}^{-1}$ ) lines, we checked this spectrum again. We cannot confirm that the line is detected. We conclude that  $\text{Ly}\alpha/\text{CIV} \gtrsim 5$  and  $\text{Ly}\alpha/\text{HeII} \gtrsim 5$ .

- 2104-242 at  $z = 2.49$  (based on VLT FORS long slit spectroscopy, Overzier et al. 2001)

- 0140+3253 at  $z = 4.41$ . According to DB01, CIV is detected and  $\text{Ly}\alpha/\text{CIV} = 43 \pm 10$ . Because of the strong sky residuals in the CIV region, we have checked the spectrum again. We cannot confirm the detection of the line. We have measured upper limits for both CIV and HeII. We obtain  $\text{Ly}\alpha/\text{CIV} \gtrsim 30$  and  $\text{Ly}\alpha/\text{HeII} \gtrsim 10$ .

- Upper limits for CIV and/or HeII were measured for 0231+3600 ( $z = 3.08$ ), 0040+3857 ( $z = 2.61$ ), 2355-002 ( $z = 2.59$ ) and 2254+185 ( $z = 2.15$ ) using the original spectra of DB01.

## 3 MODELS

Photoionization models were computed using the multipurpose code Mappings 1c (Binette, Dopita & Tuohy 1985, Ferruit et al. 1997). The following assumptions will be applied unless stated otherwise: the ionizing continuum is a power law (PL) of index  $\alpha = -1.5$  ( $F_\nu \sim \nu^\alpha$ ) with a cut off energy of  $5 \times 10^4 \text{ eV}$ . The gas is characterized by a density  $n = 100 \text{ cm}^{-3}$  and solar abundances. The clouds are radiation bounded and the geometry is plane parallel. The density behaviour within the clouds is isobaric. Dust reddening effects have been ignored in the modeling. These are the standard models which, in general, reproduce most of the UV and optical line ratios of HzRG rather successfully (e.g. Robinson et al. 1987, Villar-Martín et al. 1997, Humphrey 2005).

| Object           | $z$  | Ly $\alpha$ /HeII          | Ly $\alpha$ /CIV | P(%)           | $S_{850\mu m}$ (mJy) |
|------------------|------|----------------------------|------------------|----------------|----------------------|
| <b>0140+3253</b> | 4.41 | $\gtrsim 10$               | $\gtrsim 30$     | –              | 3.3 $\pm$ 1.5        |
| <b>1338-1941</b> | 4.11 | <b>18<math>\pm</math>4</b> | 11 $\pm$ 2       | 5.0            | 7 $\pm$ 1            |
| 4C60.07          | 3.79 | –                          | 3.7              | –              | 17 $\pm$ 1           |
| <b>4C41.17</b>   | 3.79 | <b>27<math>\pm</math>2</b> | 11.1 $\pm$ 0.7   | <2.4           | 12.1 $\pm$ 0.9       |
| <b>1911+6342</b> | 3.59 | <b>18<math>\pm</math>2</b> | 18 $\pm$ 2       | –              | <11.9                |
| <b>2141+192</b>  | 3.59 | <b>17.8</b>                | 10.6             | –              | <5                   |
| <b>1243+036</b>  | 3.57 | <b>34<math>\pm</math>3</b> | 14 $\pm$ 1       | 11 $\pm$ 4     | <6.5                 |
| 0121+1320        | 3.52 | 7.1 $\pm$ 2                | 8 $\pm$ 2        | 7 $\pm$ 2      | 7.5 $\pm$ 1.0        |
| <b>0205+2242</b> | 3.51 | <b>26<math>\pm</math>4</b> | 18 $\pm$ 2       | –              | <5.2                 |
| 0902+34          | 3.40 | 9.1                        | 6.3              | 1.5            | –                    |
| 1123+314         | 3.22 | 2.6 $\pm$ 0.4              | 1.8 $\pm$ 0.3    | –              | 5 $\pm$ 1            |
| 1112-2948        | 3.09 | 2.4 $\pm$ 0.3              | 4.1 $\pm$ 0.7    | –              | 5.9 $\pm$ 1.6        |
| 0231+3600        | 3.08 | $\gtrsim 5$                | $\gtrsim 5$      | –              | 6 $\pm$ 2            |
| 0747+365         | 2.99 | 3.5 $\pm$ 0.7              | 4.6 $\pm$ 0.9    | –              | 5 $\pm$ 1            |
| 0943-242         | 2.92 | 7.4                        | 5.2              | 6.6 $\pm$ 0.9  | –                    |
| 4C24.28          | 2.88 | –                          | 4.3              | –              | 2.4 $\pm$ 1.2        |
| 0857+036         | 2.81 | 3.7                        | 2.6              | –              | –                    |
| 0417-181         | 2.77 | 6.0                        | 2.5              | –              | –                    |
| 1019+0534        | 2.77 | 1.0                        | 0.8              | –              | <3.8                 |
| 1338+3532        | 2.77 | 5.9 $\pm$ 0.8              | 14 $\pm$ 3       | –              | –                    |
| <b>0920-071</b>  | 2.76 | <b>15<math>\pm</math>2</b> | 12 $\pm$ 2       | –              | –                    |
| 1545-234         | 2.76 | 3.7                        | 6.1              | –              | –                    |
| 2202+128         | 2.71 | 3.2                        | 4.1              | –              | –                    |
| 1357+007         | 2.67 | –                          | 5.4              | –              | –                    |
| 0040+3857        | 2.61 | $\gtrsim 5$                | 4 $\pm$ 2        | –              | –                    |
| 2355-002         | 2.59 | $\gtrsim 3$                | 4.0 $\pm$ 1      | –              | –                    |
| 0529-549         | 2.58 | 12.3                       | 18.5             | –              | –                    |
| 0828+193         | 2.57 | 7.0                        | 7.0              | 10 $\pm$ 1     | –                    |
| <b>1755-6916</b> | 2.55 | <b>23<math>\pm</math>4</b> | 15 $\pm$ 2       | –              | –                    |
| 1436+157         | 2.54 | 7.0                        | 2.5              | –              | –                    |
| 1558-003         | 2.53 | 8.8                        | 5.5              | –              | –                    |
| <b>0303+3733</b> | 2.51 | <b>21<math>\pm</math>4</b> | 7 $\pm$ 1        | –              | –                    |
| 1650+0955        | 2.51 | 8 $\pm$ 1                  | 7 $\pm$ 1        | –              | –                    |
| 2104-242         | 2.49 | 10 $\pm$ 1                 | 13 $\pm$ 2       | –              | –                    |
| 2334+1545        | 2.48 | $\gtrsim 5$                | $\gtrsim 5$      | –              | –                    |
| 4C23.56          | 2.48 | 5.3                        | 3.8              | 15 $\pm$ 2     | <5.5                 |
| 2308+0336        | 2.46 | 7.5                        | 4.7              | –              | <3.2                 |
| <b>0731+438</b>  | 2.43 | <b>14<math>\pm</math>1</b> | 8.6 $\pm$ 0.7    | <2.4           | –                    |
| 1033-1339        | 2.43 | 12 $\pm$ 2                 | 4.3 $\pm$ 0.7    | –              | –                    |
| 0748+134         | 2.42 | 4.2                        | 3.5              | –              | –                    |
| 1410-001         | 2.36 | 11.1                       | 8.3              | 12 $\pm$ 3     | –                    |
| 1707+105         | 2.35 | 4.8                        | –                | –              | –                    |
| 0128-264         | 2.35 | –                          | 7.2              | –              | –                    |
| 1428-1502        | 2.35 | 9 $\pm$ 2                  | 9 $\pm$ 2        | –              | –                    |
| 4C48.48          | 2.34 | 11 $\pm$ 1                 | 8.2 $\pm$ 0.8    | 8.4 $\pm$ 1.5  | 5 $\pm$ 1            |
| 0211-122         | 2.34 | 1.0                        | 1.8              | 19 $\pm$ 1     | –                    |
| 1251+1104        | 2.32 | 7.7                        | 7.7              | –              | –                    |
| 4C40.36          | 2.27 | 11.6 $\pm$ 0.8             | 7.3 $\pm$ 0.7    | 7 $\pm$ 1      | <4.1                 |
| 1113-178         | 2.24 | 9.1                        | 3.8              | –              | –                    |
| 0200+015         | 2.23 | 5.4                        | 4.1              | –              | –                    |
| 1138-262         | 2.16 | 10.7                       | 17.4             | –              | 13 $\pm$ 3           |
| 0355-037         | 2.15 | 3.0                        | 4.1              | –              | –                    |
| 2254+185         | 2.15 | 10 $\pm$ 5                 | $\gtrsim 4.0$    | $\lesssim 2.6$ | –                    |
| 2036+0256        | 2.13 | 10 $\pm$ 3                 | 11 $\pm$ 5       | –              | –                    |
| 1102-1651        | 2.11 | 2.1 $\pm$ 0.5              | 2.7 $\pm$ 0.7    | –              | –                    |
| 1802+645         | 2.11 | –                          | 8.9              | –              | –                    |
| 1740+664         | 2.10 | –                          | 13.7             | –              | –                    |
| 0448+091         | 2.04 | 8.7                        | 10.1             | –              | –                    |
| 1805+633         | 1.84 | –                          | 6.8              | –              | –                    |
| 3C256            | 1.82 | 9.9                        | 10.4             | 12 $\pm$ 2     | –                    |
| 3C294            | 1.79 | 10                         | 10               | –              | <2.3                 |

**Table 1.** Sample of radio galaxies used in this study in order of decreasing redshift and with some relevant information. LAEs are highlighted in bold.  $z \geq 3$  and  $z < 3$  radio galaxies are separated by a horizontal line. See §2 for references of the optical data. P(%) values are from Vernet et al. 2001, Dey et al. 1997, De Breuck et al. (in prep.) and Jannuzi et al. 1995. Submm data are from Archibald et al. 2001 and Reuland et al. 2004. No available measurements are indicated with ‘–’. Errors for P(%) and  $S_{850}$  are provided when available.

All the stellar SEDs (Spectral Energy Distributions) used in this paper were built using Starburst99 (Leitherer et al. 1999), a web based software and data package designed to model spectrophotometric and related properties of star-forming galaxies. We have assumed an initial mass function (IMF) with spectral indexes 1.3 and 2.3 for the mass intervals 0.1 to 0.5  $M_{\odot}$  and 0.5 to 120  $M_{\odot}$  respectively. Stellar abundances are always considered to be solar. Both continuous and instantaneous star forming histories were considered.

#### 4 VARIATION OF $\text{Ly}\alpha/\text{HeII}$ , $\text{Ly}\alpha/\text{CIV}$ AND $\text{Ly}\alpha$ LUMINOSITY WITH REDSHIFT

In this section we investigate how the  $\text{Ly}\alpha/\text{HeII}$  and  $\text{Ly}\alpha/\text{CIV}$  ratios and the  $\text{Ly}\alpha$  luminosity change with redshift. Both ratios have been measured in many radio galaxies at  $z \gtrsim 2$ , since the lines are observable in the optical window.

Three diagnostic diagrams involving the  $\text{Ly}\alpha$ , HeII and CIV lines are shown in Fig.1. The solid line represents standard photoionization models (see §3). The ionization parameter  $U^1$  varies within the range [0.0046,1].

The  $\text{Ly}\alpha/\text{HeII}$  ratio predicted by the models is in the range  $\sim 15$ -20. Due to its strong sensitivity to  $U$ , the predicted  $\text{Ly}\alpha/\text{CIV}$  values cover a much larger range. The minimum predicted value is  $\sim 9$ . Because  $\text{Ly}\alpha/\text{HeII}$  shows little dependence on  $U$  compared with  $\text{Ly}\alpha/\text{CIV}$ , we will focus most of our discussion on the first ratio, with reference to other ratios when useful.

All objects in Table 1 with measurements available for the three line ratios (including lower and upper limits) are plotted in Fig. 1. We have marked with coloured symbols those radio galaxies with  $\text{Ly}\alpha/\text{HeII}$  values consistent with or above the standard case B value (0140+3253 at  $z = 4.41$  is the only exception, see below). Given that errors are not available for many radio galaxies in the sample, we consider an object to be consistent with the model predictions when  $\text{Ly}\alpha/\text{HeII}$  is at least 90% of the minimum values predicted by the models, i.e.  $\text{Ly}\alpha/\text{HeII} \geq 14$ . Because of the very high values compared with typical values of most HzRG, we will call these radio galaxies  $\text{Ly}\alpha$  excess objects (LAEs hereafter). Black symbols correspond to objects with  $\text{Ly}\alpha/\text{HeII}$  ratios below the case B recombination value.

The diagrams show a very clear segregation of the most distant radio galaxies in the sense that most  $z \geq 3$  objects have the highest  $\text{Ly}\alpha/\text{HeII}$  values. The  $\text{Ly}\alpha/\text{CIV}$  ratios of these objects are also among the largest values.

Of the 10 sources at  $z \geq 3$  for which  $\text{Ly}\alpha/\text{HeII}$  has been measured, 6 have  $\text{Ly}\alpha/\text{HeII} \geq 14$  and are therefore LAEs. 4 are not LAEs. It is not possible to classify the remaining three  $z \geq 3$  radio galaxies due to the unavailability of the  $\text{Ly}\alpha/\text{HeII}$  value.

One more  $z \geq 3$  radio galaxy can be added to the group of LAEs: 0140+3253 ( $z = 4.41$ ), which shows  $\text{Ly}\alpha/\text{HeII} \gtrsim 10$  and  $\text{Ly}\alpha/\text{CIV} \gtrsim 30$ . The large  $\text{Ly}\alpha/\text{CIV}$  ratio does not necessarily imply that the object is a LAE, since this ratio can

be reproduced by very low or high  $U$  values (see Fig. 1). The real value of  $\text{Ly}\alpha/\text{HeII}$  would be necessary. However, the fact that this object presents the largest  $\text{Ly}\alpha/\text{CIV}$  value of the whole sample suggests that this is also a LAE in the sense that the  $\text{Ly}\alpha$  emission is unusually enhanced. This is also suggested by its high  $\text{Ly}\alpha$  luminosity ( $1.35 \times 10^{44}$  erg  $\text{s}^{-1}$ ), which is more characteristic of LAEs than non LAEs (see below). Therefore, we classify 0140+3253 as a LAE.

We conclude that at least 7 out of 13 (54%)  $z \geq 3$  radio galaxies are LAEs. On the other hand, only 4 out of 48 (8%)  $2 \lesssim z < 3$  radio galaxies can be classified as such (see Table 1)<sup>2</sup>.

We show in Table 2 the median and average (1st number in brackets) values of the  $\text{Ly}\alpha$  ratios for the two redshift samples together with other interesting information (upper and lower limits have been excluded in the calculations).  $\text{Ly}\alpha/\text{HeII}$  and  $\text{Ly}\alpha/\text{CIV}$  are  $\sim 2.2$  and  $\sim 1.5$  times larger in  $z \geq 3$  radio galaxies, which also tend to have noticeably larger  $\text{Ly}\alpha$  ( $\sim 3$  times) luminosities compared with the low  $z$  sample. The CIV/HeII ratio is similar in both groups. The bottom line shows the probabilities  $P$  that the two groups are drawn from different parent populations according to the Kolmogorov-Smirnov test. These values confirm that  $z \geq 3$  radio galaxies show larger  $\text{Ly}\alpha$  ratios and higher  $\text{Ly}\alpha$  luminosities. Interestingly, there is no distinction in radio size between the two samples.

We have repeated the calculations from Table 2, this time separating the sample into LAE and non-LAE sources, rather than into  $z < 3$  and  $z \geq 3$  sources. The results are shown in Table 3. LAEs tend to be at higher redshift with a median  $z$  value  $z_{med} = 3.57$ , while  $z_{med} = 2.48$  for objects with no  $\text{Ly}\alpha$  excess. They have  $\text{Ly}\alpha$  luminosities  $\sim 3.4$  times higher and  $\text{Ly}\alpha/\text{HeII}$  and  $\text{Ly}\alpha/\text{CIV}$  ratios 2.7 and 2.1 times higher respectively compared with non-LAEs. Interestingly, also the CIV/HeII ratio is 1.6 times higher. There is also a clear difference in radio size. The bottom line shows the  $P$  values resulting from the Kolmogorov-Smirnov test.

Interestingly, there are 4 LAEs (out of 11, i.e. 36%) which, even after taking into account the errors, show a  $\text{Ly}\alpha/\text{HeII}$  well *above* the maximum value (20) predicted by the models. These objects are: 1338-1941 ( $\text{Ly}\alpha/\text{HeII} \sim 30$  once corrected for absorption, Wilman et al. 2004), 4C41.17, 1243+036, 0205+2242, all at  $z > 3$ . No or very weak absorption has been found for the LAEs 4C41.17, 1243+036 (van Ojik et al. 1997) and 1755-6916 (Wilman et al. 2004). This information is not available for the rest of the LAEs.

#### 4.1 Measurements of spatially extended $\text{Ly}\alpha$ ratios

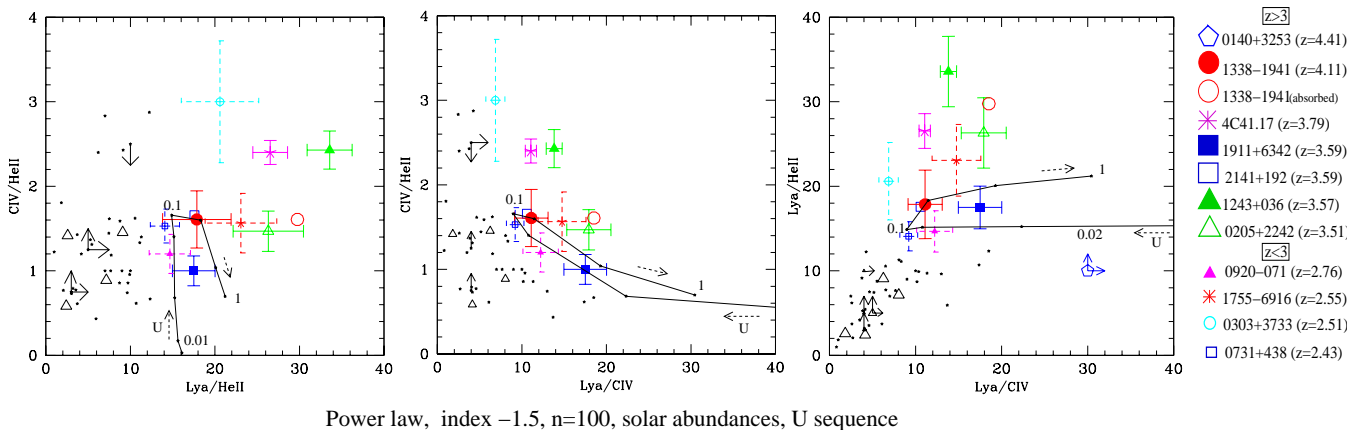
The results above are based on spatially integrated spectra, centered on the high surface brightness regions (although not necessarily covering the whole extension of the emission line regions). There are two  $z \geq 3$  objects in the literature for which the spatial variation of the  $\text{Ly}\alpha$  ratios has been

<sup>1</sup>  $U = \frac{Q}{4\pi r^2 n c}$ , where  $Q$  is the photon ionizing luminosity,  $r$  is the distance between the cloud and the ionizing source,  $n$  is the particle gas density and  $c$  is the speed of light.

<sup>2</sup> Considering a power law of index  $\alpha = -1.0$  (Villar-Martín, Tadhunter & Clark, 1997) would not change our conclusions.  $\text{Ly}\alpha/\text{HeII}$  would be in the range  $\sim 10$ -14, implying that still the vast majority of  $2 \lesssim z < 3$  objects lie below the model predictions, while most  $z \geq 3$  radio galaxies are LAEs.

| $z$ range          | $\frac{Ly\alpha}{HeII}$ | $\frac{Ly\alpha}{CIV}$ | $\frac{CIV}{HeII}$ | $L(Ly\alpha)$<br>$10^{44} \text{ erg s}^{-1}$ | LAS                |
|--------------------|-------------------------|------------------------|--------------------|---|--------------------|
| $2 \lesssim z < 3$ | 8.00 (8.32,[4.75])      | 6.90 (7.24,[4.21])     | 1.20 (1.29,[0.65]) | 0.44 (0.74,[0.79])                            | 52 (66.2,[60.6])   |
| $z \gtrsim 3$      | 17.50 (16.01,[10.90])   | 10.60 (10.07,[5.41])   | 1.44 (1.51,[0.59]) | 1.35 (1.34,[1.03])                            | 43.0 (78.0,[74.7]) |
| $P$                | 99%                     | 96.5%                  | 71%                | 93%   | 1%                 |

**Table 2.** The median, average (first number in brackets) and standard deviation (2nd number in brackets) of the main UV line ratios and the  $Ly\alpha$  luminosities in the  $2 \lesssim z < 3$  and  $z \gtrsim 3$  samples are shown. The  $Ly\alpha/HeII$  and  $Ly\alpha/CIV$  ratios are  $\sim 2.2$  and  $1.5$  times higher in the  $z \gtrsim 3$  sample. On the other hand,  $Ly\alpha$  is  $\sim 3$  times more luminous in this sample. No distinction is apparent on radio size between the two samples. The bottom line shows the probability that the two samples are drawn from different parent populations according to the Kolmogorov-Smirnov test. (Radio largest angular size values (LAS, in Tables 2 and 3) taken from DB01, DB00a and De Breuck et al. 2000b)



Power law, index  $-1.5$ ,  $n=100$ , solar abundances, U sequence

**Figure 1.** Diagnostic diagrams involving the  $Ly\alpha$ , HeII and CIV emission lines (see electronic manuscript for colour version of the figures). The solid black line represents the standard  $U$  sequence of photoionization models (see text), with the  $U$  value indicated for some points along the sequence. The dashed arrows show the sense of increasing  $U$ . The  $Ly\alpha/HeII$  values predicted by the models are in the range  $\sim 15$ - $20$ . Objects with  $Ly\alpha/HeII$  ratios consistent with or above such values (named LAEs throughout this work) are indicated in colour and their names shown in the adjacent labels. Error bars for these objects are shown when available. Radio galaxies at  $z < 3$  are shown with dashed errorbars and/or small sized symbols and radio galaxies at  $z \gtrsim 3$  are shown with solid errorbars and/or large sized symbols. Solid arrows indicate lower and upper limits. The  $Ly\alpha$  ratios have not been corrected for absorption effects, except for 1338-192 for which both the absorbed (red solid circle) and corrected (red hollow circle) values are shown. The  $z \gtrsim 3$  sample tend to have larger  $Ly\alpha/HeII$  and  $Ly\alpha/CIV$  ratios.  $Ly\alpha/HeII$  is above the model predictions for several objects.

investigated in the direction of the radio structures (both of them are in the sample above): 1243+036 (green solid triangle in the figures) at  $z = 3.36$  (Humphrey 2005, Humphrey et al. 2006, in prep.) and 2141+192 (blue open square in the figures) at  $z = 3.59$  (Maxfield et al. 2002). For 1243+036 the  $Ly\alpha/HeII$  ratio has values in the range  $26 \pm 5$  up to  $\gtrsim 40$  in the outer parts ( $\gtrsim 7''$  from the nuclear region) of the object.  $Ly\alpha/HeII = 33 \pm 1$  in the nuclear region. On the other hand,  $Ly\alpha/CIV$  presents a minimum in the nuclear region ( $14 \pm 1$ ) and a maximum of  $\gtrsim 40$  (this is a lower limit) in the outer parts of the object ( $\gtrsim 7''$ ). The spatially integrated values are  $\sim 34 \pm 1$  and  $14 \pm 1$  respectively.

The second object is 2141+192 at  $z = 3.59$  (Maxfield et al. 2002). The integrated spectrum gives  $\sim 18$  and  $11$  for  $Ly\alpha/HeII$  and  $Ly\alpha/CIV$  respectively. Fig. 7 in Maxfield et al. (2002) shows a region at  $\sim 1.5''$  from the continuum centroid, where  $Ly\alpha/HeII \gtrsim 40$  and  $Ly\alpha/CIV \sim 15$ - $20$ . At  $\sim 4$ - $4.5''$ ,  $Ly\alpha/HeII \gtrsim 30$ .

Humphrey (2005) (Humphrey et al. 2006, in prep.) studied the spatial variation of the  $Ly\alpha$  ratios for a sample of 10 radio galaxies (all included in our study) in the redshift range  $2 < z < 3$ . Five of these objects (1558-003, 4C40.36, B3 0731+438, 4C48.48 and 4C-00.54) show  $Ly\alpha/HeII$  in the range 14-30 at some spatial positions in the extended gas. These large  $Ly\alpha/HeII$  values are measured in all cases outside the nuclear region. Among these five objects, only B3 0731+438 is classified as a LAE from its spatially integrated spectrum (blue hollow small square in the figures).

## 5 SCENARIOS

In this section, we will investigate *a)* why  $Ly\alpha$  is unusually strong in LAEs relative to other emission lines and the continuum, compared with the majority of HzRG; *b)* why

| Object class | $z$                | $\frac{Ly\alpha}{HeII}$ | $\frac{Ly\alpha}{CIV}$ | $\frac{CIV}{HeII}$ | $L(Ly\alpha)$<br>$10^{44} \text{ erg s}^{-1}$ | LAS<br>kpc         |
|--------------|--------------------|-------------------------|------------------------|--------------------|---|--------------------|
| non-LAEs     | 2.48 (2.53,[0.42]) | 7.25 (6.94,[3.30])      | 5.45 (6.70,[4.05])     | 1.00 (1.20,[0.60]) | 0.43 (0.77,[0.84])                            | 85.2 (53.5,[74.7]) |
| LAEs         | 3.57 (3.35,[0.68]) | 19.50 (21.38,[6.20])    | 11.50 (12.52,[3.69])   | 1.63 (1.80,[0.62]) | 1.45 (1.55,[1.05])                            | 18.5 (38.8,[42.6]) |
| $P$          | 98%                | –                       | 99.9%                  | 99.5%              | 94%   | 90%                |

**Table 3.** As Table 2, but the objects have been classified as LAEs (radio galaxies with Ly $\alpha$  excess) and non-LAEs. The LAEs tend to be at higher redshift. Ly $\alpha$  is  $\sim 3.4$  times more luminous in these objects and the Ly $\alpha$ /HeII and Ly $\alpha$ /CIV ratios are 2.7 and 2.1 times higher than in non-LAEs. The radio size is  $\sim 4.6$  times smaller for LAEs. The bottom lines shows the  $P$  values resulting from the Kolmogorov-Smirnov test.

LAEs show Ly $\alpha$ /HeII values which are often well above the standard model predictions (see §4).

We are looking for a mechanism that can enhance the Ly $\alpha$  emission over other emission lines and the continuum. We have considered two possibilities: different properties of the ionized nebulae (heavy element abundances, gas density, absorption and scattering properties) and alternative ionization mechanisms (shocks, stellar photoionization vs. AGN photoionization).

The diagrams in Fig. 1 show a large scatter of the measured Ly $\alpha$  ratios, which cannot be explained by the standard models. Most radio galaxies show too faint Ly $\alpha$  relative to CIV and HeII. The most natural explanation is that the Ly $\alpha$  photons are absorbed by neutral gas and dust. Therefore, the most realistic way to model the line ratios of the *whole sample* should take absorption effects into account. This information is available only for a few objects (Wilman et al. 2004). Van Ojik et al. (1997) found clear signs of absorption in 11 out of 18 radio galaxies at  $z \gtrsim 2$ , but they do not provide the information necessary to correct the Ly $\alpha$  fluxes in the absorbed objects.

Our expectation is that LAEs should show stronger absorption than non LAEs. DB00a found that Ly $\alpha$  absorption occurs most frequently in sources with small radio sources (see also van Ojik et al. 1997) and at higher redshifts. Since most LAEs have higher  $z$  and smaller radio sizes than non LAEs (see Table 3), it is likely that they are also more absorbed. In this case, they are likely to be more overluminous in Ly $\alpha$  than assumed in this work.

On the other hand, the goal of this study is to explain the Ly $\alpha$  excess in the LAEs. For this and the above reason, absorption will be ignored in our models, but only discussed qualitatively when necessary. It is, therefore, not to be expected that the models presented in this section should reproduce the line ratios of the whole sample, but only those of the LAEs.

### 5.1 Lower metallicities.

We investigate next whether lower nebular metallicities in LAEs can explain the observational results.

A decrease of the heavy element abundances will enhance the nebular electron temperature, which will favour the collisional excitation of Ly $\alpha$  (and heavy element lines such as CIV $\lambda$ 1550), while this process will not affect HeII $\lambda$ 1640 or the continuum significantly.

We have computed a set of photoionization models to investigate the impact of the metallicity variation on the Ly $\alpha$  ratios. The density has been fixed to  $n=100 \text{ cm}^{-3}$ . We

show in Fig. 2 the same diagnostic diagrams as before, with two model sequences for  $U=0.05$  (dashed black line) and  $U=0.015$  (red solid line) respectively. A range of  $U$  values is considered, since the ionization level of the gas is known to vary from object to object (i.e., Robinson et al. 1987, Villar-Martín et al. 1997, Humphrey 2005). The metallicity range covered by the two sequences is 0.05 to  $2 Z_{\odot}$ .  $U$  values outside the quoted range would produce *a)* similar results ( $U=0.1$  would produce similar results to  $U=0.05$ , although implying even lower metallicities for the objects) or *b)* discrepant line ratios. For example, very low ionization models ( $U \lesssim 0.005$ ) produce too faint CIV emission so that CIV/HeII $<0.4$ . On the contrary, very high ionization models ( $U \gtrsim 0.3$ ) which can explain Ly $\alpha$ /HeII $\gtrsim 25$  predict too strong CIV, with CIV/HeII $\gtrsim 4$ .

As the metallicity decreases towards well below solar values, the UV line ratios (in particular Ly $\alpha$ /HeII) change dramatically. For  $Z \gtrsim 50\% Z_{\odot}$  this ratio is rather constant, since the nebula is too cold to produce any noticeable collisional excitation of Ly $\alpha$ . As the metallicity decreases further, the high electron temperature makes this mechanism very efficient and the Ly $\alpha$ /HeII ratio increases by a factor of 2 in the metallicity range 5-50 %  $Z_{\odot}$ . The models also succeed to reproduce the high CIV/HeII ratios for some LAEs.

A u-turn in the model sequences is observed for the ratios involving CIV due to the relatively less efficient excitation of the line (compared with Ly $\alpha$  and HeII) as the ions become more and more scarce as the metallicity decreases. Interestingly, metallicities as low as 5% still produce strong metal (CIV) lines relative to HeII, with CIV/HeII $>1$  if the gas is highly ionized ( $U \sim 0.05-0.1$ ).

5 LAEs are consistent with solar abundances, choosing the appropriate  $U$  value and taking errors into account (lower metallicities are not discarded, though, due to the  $U$ - $Z$  degeneracy in this area of the diagrams). These objects are: 1911+6342, 2141+192 and 1338-1941 at  $z > 3$  and 0920-071, 0371+438 at  $z < 3$ . Once corrected for Ly $\alpha$  absorption, one of them (1338-1941, red circles) shifts towards the low metallicity models (10%  $Z_{\odot}$ ). I.e. if absorption was taken into account, it is possible that more objects would require well below solar abundances.

Including 1338-1941, 6 LAEs have  $Z \lesssim 25\% Z_{\odot}$  according to their UV line ratios. Interestingly, very low abundances  $Z \lesssim 10\% Z_{\odot}$  are inferred for 4 of these objects: 1338-1941, 1243+036, 4C41.17, 1338-1941 (once corrected for absorption) and 0205+2242, all at  $z > 3$ .

According to these results, LAEs are, on average, characterized by lower abundances than radio galaxies with no Ly $\alpha$  excess. Abundances of less than 25%  $Z_{\odot}$  are implied in

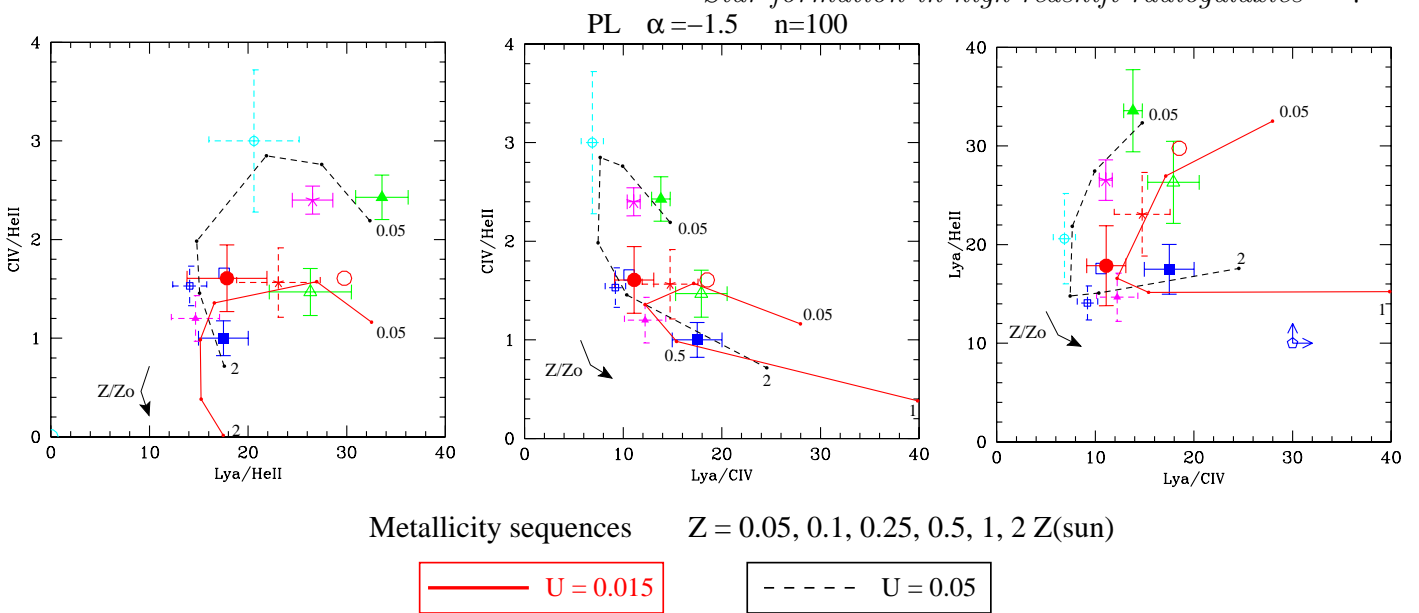


**Figure 2.** Metallicity effects. Same diagnostic diagrams as in Fig.1. The black and red lines represent sequences of photoionization models for two different  $U$  values. The metallicity varies in the range 0.05 to 2  $Z_{\odot}$  in both cases. The black arrows indicate the sense of increasing metallicity. Metallicity effects are very successful at reproducing the position of LAEs in these three diagnostic diagrams. Notice that at least 7 out of 13 objects require abundances  $\lesssim 25\% Z_{\odot}$ . However, the models fail to reproduce the strength of the NV emission in at least the most extreme LAEs (see text).

$\sim 55\%$  of LAEs. Since  $\text{Ly}\alpha$  absorption has been taken into account for only one object, the metallicities could be even lower.

The  $\text{NV}\lambda 1240$  line provides a strong test for the validity of the low metallicity scenario. According to the models, this line should be very faint in the most metal poor objects. Its flux has been measured in three of them: 1243+036, 4C41.17 and 1338-1992. We show in Table 4 the predictions of the  $\text{NV}/\text{HeII}$  and  $\text{NV}/\text{CIV}$  ratios for the models that best reproduce the  $\text{Ly}\alpha$  ratios of these three objects, together with the measured values. It is clear that in all three cases the NV emission is observed to be much (2 to 4 times) stronger than expected from the model predictions. Nitrogen overabundance has been frequently found in different types of objects. This is usually attributed to secondary production of nitrogen. However, this mechanism cannot work at the very low metallicities implied by the models (Vila-Costas & Edmunds 1993). Therefore, these LAEs are unlikely to have low metallicities.

We therefore conclude that low metallicities do not provide a satisfactory explanation for at least the most extreme LAEs.

## 5.2 Density enhancement.

An efficient way to enhance  $\text{Ly}\alpha$  over other emission lines and the continuum is increasing the gas density. At low densities the cooling of the nebula is due mostly to some forbidden lines (e.g.  $[\text{OIII}]\lambda 4959, 5007$ ,  $[\text{OII}]\lambda 3727$ , etc), via radiative de-excitation of their upper energy levels in the original ion. As the density increases, the critical density will be reached for some of these transitions, so that de-excitation becomes collisional, rather than radiative and radiative cooling becomes much less efficient. The electron temperature

rises as a consequence and  $\text{Ly}\alpha$  will have an increasing contribution of collisional excitation in the partially ionized zone, which does not affect the  $\text{HeII}\lambda 1640$  recombination line.

In addition, when densities approach values  $\sim 10^5 \text{ cm}^{-3}$ , the fraction of energy emitted as  $\text{Ly}\alpha$  photons versus two-photon continuum emission due to the decay of the  $2^2\text{S}$  level of H tends toward unity, rather than 0.67 at the low density limit (Binette et al. 1993).

The dramatic increase of  $\text{Ly}\alpha/\text{HeII}$  with density can be clearly seen in Fig. 3, where the red-solid and black-dashed lines are sequences of photoionization models for two different  $U$  values (solid red line:  $U=0.05$ ; black dashed line:  $U=0.7$ ), with  $n$  varying along each sequence in the range  $10^{1-7} \text{ cm}^{-3}$  and  $10^{1-6} \text{ cm}^{-3}$  respectively. CIV collisional excitation is also more efficient so that  $\text{CIV}/\text{HeII}$  increases dramatically with density, while  $\text{Ly}\alpha/\text{CIV}$  decreases.

Fig. 3 shows that density effects (coupled with a variation in  $U$ ) can explain the location of all LAEs in the diagnostic diagrams (intermediate  $U$  values would lie between the two sequences). It is important to note that high densities not only help to reproduce large  $\text{Ly}\alpha/\text{HeII}$  ratios, but also the trend for LAEs to show larger  $\text{CIV}/\text{HeII}$ , well above standard model predictions in some cases (see Fig.1). There are however arguments that make this explanation fail.

The implied densities for some LAEs (e.g. 1243+036 and 4C41.17) are  $\sim 10^5 \text{ cm}^{-3}$ , i.e. very high compared with the densities measured or inferred for the extended emission line regions of radio galaxies at all redshifts ( $\lesssim$  several to few hundred  $\text{cm}^{-3}$ ). On the other hand, such high densities exist in the nuclear narrow line region (e.g. De Robertis & Osterbrock 1984).

Is it possible that the emission line spectrum of LAEs is dominated by the high density nuclear gas? This could be the case for one of them, 1338-1941 ( $z=4.11$ ,  $\text{Ly}\alpha/\text{HeII}\sim 30$ ,

| Object                 | $\frac{Ly\alpha}{HeII}_{obs}$ | $\frac{Ly\alpha}{CIV}_{obs}$ | $\frac{NV}{HeII}_{obs}$ | $\frac{NV}{CIV}_{obs}$ | $(U, Z)_{mod}$            | $\frac{Ly\alpha}{HeII}_{mod}$ | $\frac{Ly\alpha}{CIV}_{mod}$ | $\frac{NV}{HeII}_{mod}$ | $\frac{NV}{CIV}_{mod}$ |
|------------------------|-------------------------------|------------------------------|-------------------------|------------------------|---------------------------|-------------------------------|------------------------------|-------------------------|------------------------|
| 1243+036 <sup>a</sup>  | 34±3                          | 14±1                         | 0.9±0.1                 | 0.37±0.06              | (0.05, 5% $Z_{\odot}$ )   | 32.3                          | 14.8                         | 0.26                    | 0.12                   |
| 4C41.17 <sup>b</sup>   | 27±2                          | 11.1±0.7                     | 0.71±0.08               | 0.29±0.03              | (0.05, 10% $Z_{\odot}$ )  | 27.5                          | 10.0                         | 0.37                    | 0.13                   |
| 1338-1992 <sup>c</sup> | 18±4                          | 11±2                         | 0.29±0.05               | 0.18±0.02              | (0.015, 10% $Z_{\odot}$ ) | 16.6                          | 12.2                         | 0.08                    | 0.06                   |

**Table 4.** Comparison between the  $Ly\alpha/HeII$ ,  $Ly\alpha/CIV$ ,  $NV/HeII$  and  $NV/CIV$  measured (*obs*) and predicted (*mod*) values for three of the most extreme LAEs. Measurements have been taken from: <sup>a</sup>Humphrey 2005 (Humphrey et al. 2006, in prep.); <sup>b</sup>Dey et al. 1997; <sup>c</sup>De Breuck et al. (in prep.). The best model characteristic parameters  $(U, Z)_{mod}$  for each object are shown in column 6. NV is observed to be much stronger than the models predict.

once corrected for absorption), for which the two dimensional  $Ly\alpha$  spectrum appears very compact (De Breuck et al. 1999), or objects such that the aperture used to extract the spectra studied in this paper was optimized to isolate the nuclear emission. However, very high densities ( $\gtrsim 10^5$  cm<sup>-3</sup>) at large nuclear distances are implied by the enhanced  $Ly\alpha/HeII$  ratios measured in the extended gas of several objects (see §4.1).

An alternative possibility is that the gas that emits most of the line flux is distributed in very dense clumps, which can be at large distances from the nuclear region. As an example, Dey et al. (1997) find that 30% of the  $Ly\alpha$  flux in 4C41.17 comes from extranuclear clumps in the scale of a few hundred pc. However, the implied photon ionizing luminosities would be unrealistically high:  $Q \sim 10^{59-61}$  s<sup>-1</sup> for  $r \sim 10$  kpc, compared with  $\sim$ several  $\times 10^{57}$  erg s<sup>-1</sup> for  $z \gtrsim 2$  quasars (e.g. Heckman et al. 1991a).

We conclude that, in general, high densities do not provide a natural explanation for the  $Ly\alpha$  excess in LAEs.

### 5.3 Absorption and resonant scattering

The simplest explanation for the larger  $Ly\alpha$  ratios in LAEs compared with objects with no  $Ly\alpha$  excess is that the line is less absorbed. This would also explain why  $Ly\alpha$  is also more luminous and has larger equivalent widths. It does not explain, however, why  $Ly\alpha/HeII$  is above the standard model predictions in some cases.

A way to enhance  $Ly\alpha$  over other emission lines is by means of resonant scattering, with an absorbing medium distributed in very dense and compact neutral dusty clumps (Hansen & Oh 2006). In such scenario, the  $Ly\alpha$  photons can be scattered by the gaseous surface of the neutral clumps without reaching the dust. All other emission lines and continuum can penetrate the dusty cores, where they will suffer absorption. If the medium is quite clumpy, the  $Ly\alpha$  photons will be able to escape unabsorbed. This can produce a noticeable increase of the line equivalent width and the ratio relative to other lines. Villar-Martín, Binette & Fosbury (1996) proposed a similar explanation for the existence of pure  $Ly\alpha$  emitting regions in some radio galaxies. It has also been suggested by Hansen & Oh (2006) to explain the intriguing large EW  $Ly\alpha$  values measured in some Ly break galaxies. Vernet et al. (2001) also found that in order to get an efficient grey scattering that explains the continuum polarization properties of HzRG, a high contrast clumpy medium is needed.

In this scenario, the ambient medium around LAEs consists of dense neutral dusty clumps while objects with no  $Ly\alpha$  excess are surrounded by a more diffuse dusty medium

where  $Ly\alpha$  is very efficiently quenched. However, as we explain above (§5) LAEs are likely to be more strongly absorbed than non-LAEs.

### 5.4 Shocks

So far we have investigated scenarios such that the same mechanism ionizes the gas in LAEs and non-LAEs, but the nebular properties are different. An alternative possibility is that the nebulae have similar properties, but the ionizing mechanism is different in both types of objects.

Shocks could enhance the  $Ly\alpha$  emission via collisional excitation of the line, thanks to the heating effect and/or density enhancement. Two of the LAEs with the highest  $Ly\alpha$  excess (e.g. 1243+036 and 4C41.17) show, indeed, clear signs of jet gas interactions (van Ojik et al. 1996, Bicknell et al. 2000). LAEs in general tend to have small radio sizes and broad emission lines, also suggestive of jet-gas interactions (e.g. Humphrey et al. 2006, Best et al. 2001).

The median values of the  $Ly\alpha$  luminosity for LAEs and non-LAEs are  $1.45 \times 10^{44}$  and  $0.43 \times 10^{44}$  erg s<sup>-1</sup> respectively. Therefore, ignoring absorption, LAEs produce an excess of  $Ly\alpha$  luminosity given by  $L(Ly\alpha)_{exc} \sim (1.45-0.43) \times 10^{44}$  erg s<sup>-1</sup> =  $10^{44}$  erg s<sup>-1</sup>. There is, of course, a dispersion around  $L(Ly\alpha)_{exc}$ , however, in order to simplify the argumentation that follows, we will consider the above value as the characteristic  $Ly\alpha$  excess for LAEs over typical radio galaxies with no  $Ly\alpha$  excess.

If shocks are responsible for the  $Ly\alpha$  excess, it must be so that the other emission lines are not noticeably enhanced. Shock models with velocities in the range 200-1000 km s<sup>-1</sup>, solar abundances and a gas precursor density of  $n = 1$  cm<sup>-3</sup> produce  $Ly\alpha/HeII$  in the range  $\sim 25-100$  and  $Ly\alpha/CIV$  in the range  $\sim 10-100$  for certain magnetic parameter values within the range  $B = 10^{-4}-10$ , which depend on the shock velocity (Mark Allen, private communication). For shock velocities larger than 400 km s<sup>-1</sup>,  $Ly\alpha/H\beta$  is in the range 30-80. I.e., the shock cooling gas can be characterized by an emission line spectrum dominated by the  $Ly\alpha$  line.

Shock models with  $Ly\alpha/HeII$  in the range 25-35 (as measured for the most extreme LAEs, i.e. those with the highest  $Ly\alpha$  excess) produce  $Ly\alpha/H\beta \sim 35$ . Therefore, the expected  $H\beta$  luminosity from the shocked gas  $L(H\beta)_{shock}$  is  $2.9 \times 10^{42}$  erg s<sup>-1</sup>.  $L(H\beta)_{shock}$  is related to the shock velocity in the clouds  $V_w$  and the mass flow rate through the shock  $\dot{M}$  by the following equation (adapted from equation 4.4 of Dopita & Sutherland 1996):

$$L(H\beta)_{shock} = 2.8 \times 10^{37} \left[ \frac{V_w}{100 \text{ km s}^{-1}} \right]^{1.41} \frac{\dot{M}}{M_{\odot} \text{ yr}^{-1}} \text{ erg s}^{-1}$$

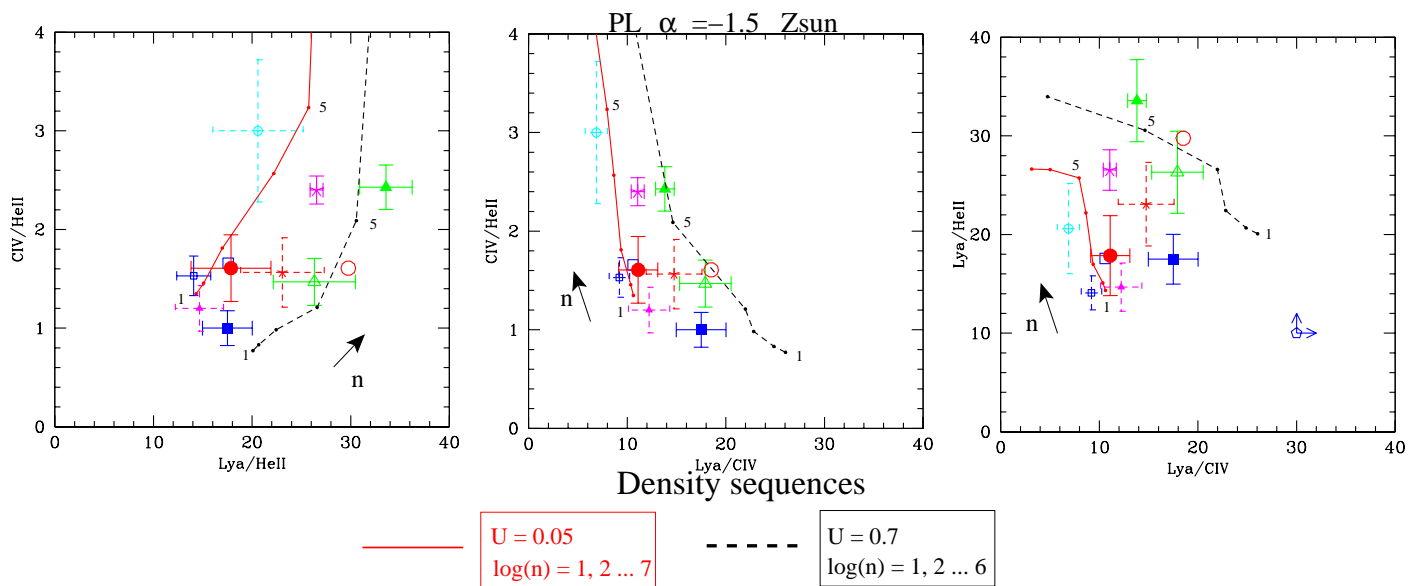


**Figure 3.** Density effects. Same diagnostic diagrams as in Fig.1 with two model sequences for different  $U$  values. Solid line:  $U = 0.05$ ; dashed line:  $U = 0.7$ . The density  $n$  varies along each sequence between  $n=10$  and  $10^7 \text{ cm}^{-3}$  or  $10^6 \text{ cm}^{-3}$  respectively. Density effects (coupled with a variation in  $U$ ) can explain the location of all LAE in the diagnostic diagrams. However, unrealistically high densities ( $n \sim 10^5 \text{ cm}^{-3}$ ) are required to reproduce the line ratios of the highest Ly $\alpha$  excess objects (see text).

Assuming  $V_w = 500 \text{ km s}^{-1}$ , this implies  $\dot{M} \sim 10^4 M_{\odot} \text{ yr}^{-1}$ . If the hot spots advance speed is in the range  $3 \times 10^3 \text{ km s}^{-1}$  (e.g. Scheuer 1995), the radio structures will need  $\sim 1.7 \times 10^{6-7} \text{ yr}$  to cross the  $\sim 50 \text{ kpc}$  radius nebulae. The total amount of material consumed in the shock will be  $\sim 1.7 \times 10^{10-11} M_{\odot}$ , which is similar or larger than the mass of the giant nebulae (e.g. McCarthy 1993, Villar-Martín et al. 2003) and is unrealistic.

If we assume that  $L(H\beta)_{\text{shock}}$  shows the same dependence on  $V_w$  for values  $> 500 \text{ km s}^{-1}$  (although we do not know whether this is the case), extreme shock velocities as high as  $V_w \gtrsim 5000 \text{ km s}^{-1}$  are required to obtain reasonable mass flow values  $\lesssim \text{several} \times 10^8 M_{\odot}$ .

The continuum emitted by the shocked gas can also photoionize the precursor gas ahead of the shock (e.g. Dopita & Sutherland 1996, Bicknell et al. 2000). However, for photoionization of the precursor to enhance Ly $\alpha$  efficiently over the other emission lines, very high densities and/or low metallicities would be required, as for standard photoionization (see above). As we discussed in §5.1 and §5.2, both scenarios have problems.

Finally, we cannot explain either why Ly $\alpha$  enhancement is not observed in the low  $z$  sample, where the extreme effects of shocks are evident in many objects (e.g. Villar-Martín et al. 2003, Humphrey et al. 2006).

We conclude that shocks do not provide a natural explanation for the Ly $\alpha$  enhancement in the LAEs.

### 5.5 Stellar photoionization

An efficient way to enhance Ly $\alpha$  over other emission lines is by means of stellar photoionization of the nebula, thanks to the soft ionizing continuum.

Assuming that 67% of the ionization processes end up in a Ly $\alpha$  photon (Binette et al. 1993),  $L(\text{Ly}\alpha)_{\text{exc}} \sim 10^{44} \text{ erg}$

$\text{s}^{-1}$  corresponds to a total ionizing luminosity of  $Q_{\text{ion}}^{\text{abs}} \sim 10^{55} \text{ s}^{-1}$  absorbed by the nebula.

A continuous burst of star formation with a star forming rate (SFR) of  $200 M_{\odot} \text{ yr}^{-1}$  produces  $Q_{\text{ion}}^{\text{mod}} = (0.9, 1.7, 2.7) \times 10^{55} \text{ s}^{-1}$  for ages of 1, 2 and 5 Myr respectively, consistent with  $Q_{\text{ion}}^{\text{abs}}$  taking into account that a fraction of the photons can escape the nebula and Ly $\alpha$  might have suffered some absorption.<sup>3</sup> Values up to a few thousands  $M_{\odot} \text{ yr}^{-1}$  in HzRG have been inferred from submm studies (e.g. Archibald et al. 2001).

Let us compare the expected continuum flux at the redshifted 1550 Å with the observed values for two of the most extreme LAEs: 4C41.17 ( $z = 3.79$ ) and 1243+036 ( $z = 3.57$ ) for which  $f_{1550} = 1.3 \times 10^{-18}$  and  $3.4 \times 10^{-19} \text{ erg s}^{-1} \text{ cm}^{-2} \text{ Å}^{-1}$  respectively in the observer's frame (Dey et al. 1997; Humphrey 2005, Humphrey et al. 2006, in prep.).

The expected monochromatic fluxes (nebular plus stellar, with the nebular component being  $\lesssim 20\%$  of the total continuum luminosity) of the bursts discussed above at the same wavelength are:  $(0.4, 0.8 \text{ and } 1.6) \times 10^{-18} \text{ erg s}^{-1} \text{ cm}^{-2} \text{ Å}^{-1}$  for 1, 2 and 5 Myr respectively at  $z \sim 3.7$ , which are consistent with the measured values.

For an instantaneous (rather than continuous) burst of star formation with the same IMF, a burst of age  $\lesssim 2 \text{ Myr}$  must have a mass  $3.8 \times 10^8 M_{\odot}$  to reproduce  $Q_{\text{ion}}^{\text{abs}}$  (older ages require larger masses). The expected monochromatic flux at 1550 Å (at  $z \sim 3.7$ ) is  $f_{1550} = 5.1 \times 10^{-19} \text{ erg s}^{-1} \text{ cm}^{-2} \text{ Å}^{-1}$  in reasonable good agreement with the continuum level of 1243+036. A mass  $\sim 10^9 M_{\odot}$  would be required to explain the continuum level of 4C41.17 (for this object, no contribution from scattered continuum is expected, Dey et al. 1997).

<sup>3</sup> The escape fraction has very uncertain values. It can vary between  $\sim 0.03$  in some nearby starburst galaxies (Leitherer et al. 1995) and  $> 0.5$  in Lyman break galaxies (Steidel, Pettini & Adelberger 2001).

It remains to be explained the trend for LAEs to show higher CIV/HeII compared with non-LAEs (median values 1.7 and 1.0 respectively, see Table 3). This ratio is well above the standard power law model predictions for several objects (see Fig.1).

A nebula photoionized by stars can be characterized by very large CIV/HeII > 1000 (Villar-Martín et al. 2004). On the other hand, provided that the gas is highly ionized, CIV can have a non-negligible flux compared with Ly $\alpha$ , with Ly $\alpha$ /CIV  $\gtrsim$  10. Therefore, the UV emission line spectrum of such a nebula will be dominated by Ly $\alpha$  and CIV, while the contribution to HeII (and NV) will be negligible. This is for instance the case of the Lynx arc, a gravitationally lensed star forming galaxy at  $z=3.36$  (Fosbury et al. 2003, Villar-Martín et al. 2004).

We show in Fig. 4 the UV line ratio predictions of models which consider an increasing contribution of stellar photoionized gas relative to the AGN ionized gas (i.e. relative to the standard power law model predictions shown in Fig. 1). The  $\omega$  parameter represents the ratio between the Ly $\alpha$  flux emitted by the stellar ionized gas and that emitted by the AGN photoionized gas. Three values have been considered  $\omega=0$  (i.e. pure AGN photoionization, black dashed line), 0.7 (red solid line) and 1.5 (green dotted line). For illustrative purposes, the stellar model predictions used here are those presented in Table 6 of Villar-Martín et al. 2004, corresponding to a single stellar age of 5 Myr and  $U=0.2$  for the stellar photoionized gas. A Salpeter IMF in the mass range 2-120  $M_{\odot}$  and an instantaneous star forming history were assumed. Ly $\alpha$ /H $\beta \sim 26$  for this model. Fig. 4 shows that a varying contribution of stellar photoionized gas to the emission line spectrum of LAEs is successful at reproducing the position of these objects in these three diagnostic diagrams.

Stellar photoionization is, therefore, a promising explanation for the Ly $\alpha$  excess in LAEs. A continuous star forming history with a star forming rate of  $\sim 200 M_{\odot} \text{ yr}^{-1}$  is very successful at explaining the excess of Ly $\alpha$  luminosity and the observed level of continuum in at least the two most extreme LAEs. Since other objects show similar continuum levels and less extreme Ly $\alpha$  excesses, it is likely that this assertion is valid for all LAEs.

45% of LAEs require  $\omega > 0$ : 1338-1941, 4C41.17, 1243+036 and 0205+224 ( $z > 3$ ) and 0303+3733 ( $z < 3$ ). The remaining LAEs are consistent with  $\omega=0$  within the errors (i.e. star formation is not required). However, since no information on the fraction of absorbed Ly $\alpha$  flux is available, except for 1755-6916 (which is not absorbed, Wilman et al. 2004),  $\omega=0$  is a lower limit.

## 6 DISCUSSION

There is additional evidence that supports stellar photoionization as the mechanism responsible for the Ly $\alpha$  excess. Fig. 5 shows Ly $\alpha$ /HeII (in log) vs.  $P(\%)$ , the polarization level of the optical continuum (UV rest frame), for all radio galaxies at  $z \gtrsim 2$  for which both have been measured (Vernet et al. 2001, Dey et al. 1997, Jannuzi et al. 1995, De Breuck et al. in prep.). There is a clear trend for objects with higher Ly $\alpha$ /HeII values to show low polarization levels. In particu-

lar, except for 1243+036, which breaks the trend, the LAEs (solid circles) show the lowest polarization levels<sup>4</sup>.

The correlation in Fig. 5 is similar to that found by Vernet et al. (2001) on a sample of radio galaxies at  $2 \lesssim z < 3$  between Ly $\alpha$ /CIV and  $P(\%)$  (all the objects in their sample are included in Fig. 5). Since the difference in polarization level between objects is most likely due to the diluting effect of young stars (Vernet et al. 2001), Fig. 5 strongly suggests that objects with higher Ly $\alpha$ /HeII ratios contain a relatively more luminous stellar population. It is important to keep in mind that the range of Ly $\alpha$ /HeII ratios must also be influenced by Ly $\alpha$  absorption (it provides a natural explanation to why this ratio is well below standard PL model predictions in some objects). However, since some LAEs need an extra supply of soft ionizing photons to enhance the Ly $\alpha$  emission, in spite of this uncertainty, Fig. 5 strongly supports that stars provide such supply.

Additional evidence for star formation has been found in several LAEs. This is the case of 4C41.17 (Dey et al. 1997, Dunlop et al. 1994, Chini & Krügel 1994) and 1338-1942 (Zirm et al. 2005). B3 0731+438, the only LAE in our study at  $z < 3$  for which optical polarization measurements exist, (Vernet et al. 2001), shows null or very low polarization level ( $< 2.4\%$ ), suggesting the presence of young stars.

De Breuck et al. (in prep.) found a tentative trend (although more objects need to be studied to confirm this result) for radio galaxies at  $z \gtrsim 3$  to show lower optical continuum polarization level than radio galaxies in the  $2 \lesssim z < 3$  range. This suggests that there is a relatively more luminous young stellar population in the highest  $z$  radio galaxies. Further evidence comes from the dramatic increase in the detection rate at submm wavelengths of  $z > 2.5$  radio galaxies ( $\sim 75\%$ ) compared with  $z < 2.5$  radio galaxies ( $\sim 15\%$ ) (Archibald et al. 2001). The authors also find that the average submm luminosity rises at a rate  $\propto (1+z)^3$  out to  $z \sim 4$ . Since most  $z > 3$  radio galaxies are LAEs, and provided that the submm emission is due to dust heated by stars (e.g. Tadhunter et al. 2005, Reuland et al. 2004) this adds further support to our interpretation that these contain more luminous young stellar populations.

Enhanced Ly $\alpha$  ratios, well above standard PL model predictions, have been measured at tens of kpc from the nucleus for the LAEs 4C41.17 and 1243+036 and some radio galaxies at  $2 \lesssim z < 3$  (§4.1), most of which are not LAEs. This suggests that star formation is spatially extended over large spatial scales. Spatially extended star formation in high  $z$  radio galaxies has been tentatively suggested by submm studies (Stevens et al. 2003). For the low  $z$  objects, although the contribution of the stars to the Ly $\alpha$  luminosity is not evident in the spatially integrated emission line spectrum, this becomes apparent at tens of kpc from the nuclear region.

Two more important issues need to be answered: Why is star formation more intense in LAEs? Was this class of objects much more common at higher ( $z \gtrsim 3$ ) redshifts and why?

<sup>4</sup> The polarization measurement for 1243+036 might not be reliable, since it could be affected by strong sky residuals. The error bar represents a statistical estimate of the error based on noise properties and possible defects due to sky residuals are not included.

## Standard PL + Stars

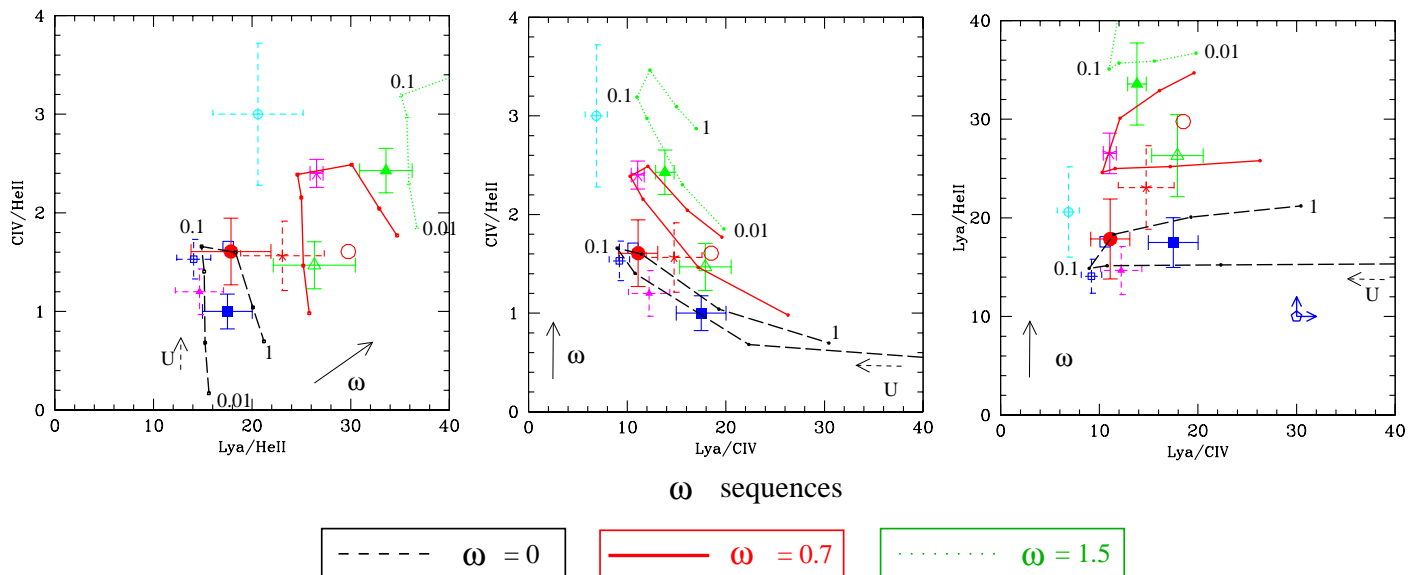


**Figure 4.** Effects on the UV line ratios due to the additional contribution of stellar photoionized gas.  $\omega = \frac{Ly\alpha_{*}}{Ly\alpha_{PL}}$  represents the ratio between the  $Ly\alpha$  flux emitted by the stellar ionized gas and that emitted by AGN ionized gas. Same diagnostic diagrams as in Fig.1. The black dashed line represents the standard PL  $U$  sequence (see Fig.1), i.e., the spectrum due to pure AGN photoionization ( $\omega=0$ ). The coloured lines represent models with an increasing contribution of emission lines from gas ionized by stars to the emission line spectrum,  $\omega=0.7$  and  $1.5$  for the red solid and green dotted lines respectively (see text for more details).  $U$  values for the PL sequence are shown for some models. The black solid arrows indicate the sense of increasing stellar contribution. A varying contribution of stellar ionized gas to the emission line spectrum of LAEs is very successful at reproducing the position of these objects in these three diagnostic diagrams.

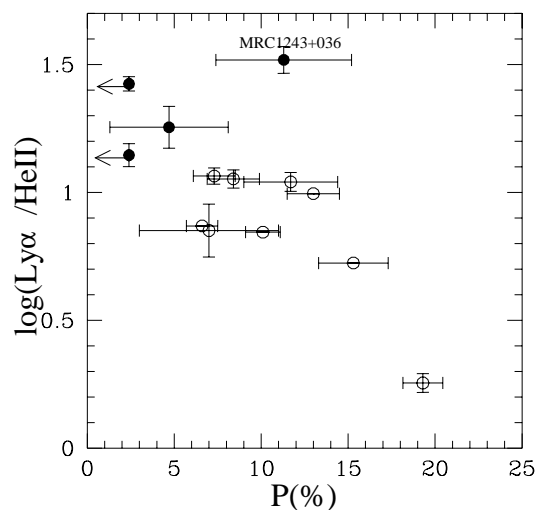


**Figure 5.**  $\log(Ly\alpha/HeII)$  vs. percentage of polarization of the optical continuum (UV rest frame) for all radio galaxies at  $z \gtrsim 2$  for which both have been measured. Black solid symbols correspond to LAEs, while hollow symbols are objects with no  $Ly\alpha$  excess. Errorbars are shown when available. Notice the clear trend for objects with the highest  $Ly\alpha/HeII$  ratios to show lower polarization, as expected if the  $Ly\alpha$  enhancement is due to stellar photoionization. The trend is broken by 1243+036, which shows too high  $P(\%)$  for its large  $Ly\alpha/HeII$  ratio (but see text).

The detailed spectroscopic study by Humphrey et al. (2006) of a sample of 10 HzRG ( $z=2-3$ ) show that small radio sources experience stronger jet-gas interactions (see also Best et al. 2001) and contain more luminous young stellar populations. This could be the case of LAEs. In fact,

this class of objects show in general broad emission lines and small radio sizes (see Table 3; De Breuck et al. (2000b), DB01, De Breuck et al. 2000b) suggestive of jet-gas interactions. These are very clear in at least two of the most extreme LAEs at  $z \gtrsim 3$ : 4C41.17 (Bicknell et al. 2000) and 1243+036 (van Ojik et al. 1996). The star formation might have been induced by the interactions, although it is not clear that this process can form enough stars to dominate the rest-frame UV emission. A more attractive possibility is that the systems have recently undergone a merger event which has triggered both the star formation and the radio/AGN activities.

According to this study, we propose to use the  $Ly\alpha$  ratios (specially  $Ly\alpha/HeII$ ) of high redshift radio galaxies and quasars to investigate the possible signature of star formation. Although these ratios have been measured for many radio galaxies at different redshifts, this has been generally done for the spatially integrated spectra, where the effect is in general less clear. We propose that the high  $Ly\alpha$  ratios relative to other emission lines found in the extended emission line regions of some high redshift radio-loud quasars (e.g. Heckman et al. 1991b) are a signature of star formation, rather than low metallicities as often proposed.

Star formation could also be responsible for the  $Ly\alpha$  emission detected in regions out of the reach of the quasar continuum and the radio structures in some high redshift radio galaxies (e.g. Villar-Martín et al. 2005, Reuland et al. 2003).

We argue next that the LAE fraction shows a genuine  $z$  evolution, not due to selection effects. Therefore, the radio galaxy phenomenon seems to have been more often associated with a massive starburst at  $z > 3$  than at  $z < 3$ .

### 6.1 Selection effects

Our results suggest that LAEs were more abundant at higher redshifts. Whether this is a genuine  $z$  evolution depends on the real fraction of LAEs at different redshifts.

An important problem we have when comparing the  $z < 3$  and  $z \geq 3$  samples are the selection effects resulting from the search techniques used to find them and the technical limitations of the spectrographs.

The parent samples were selected based on radio properties, meaning there is no a priori bias towards the optical properties. However, higher power radio sources are expected to emit stronger emission lines (Willott et al. 1999), so Malmquist bias on radio power could result on an optical bias towards strong line emitters.

Is it possible that radio power is biasing our statistics? As De Breuck et al (2000) explain, the effects of Malmquist bias in their sample is alleviated for  $2 < z < 4$ , with the addition of several filtered surveys with lower flux density limits. We have compared the radio power at 1400 MHz (rest frame frequency, DB00a) for the  $z \geq 3$  and  $z < 3$  samples (Table 5). The median, average and standard deviation  $\sigma$  are shown. According to the Kolmogorov-Smirnov test, the probability  $P$  (Table 5) that  $z \geq 3$  radio galaxies have different intrinsic radio power than the low  $z$  sample is very low (18%). So, we do not expect radio power selection criteria to introduce any bias.

Could radio size be biasing our statistics? In samples to find HzRGs, the radio size has been used as an additional high redshift filter. As we discussed above, since small radio sources tend to have more intense star formation, this selection criteria could introduce some additional bias. However, the  $2 \lesssim z < 3$  and  $z \geq 3$  samples are not different in terms of their radio sizes (see §4, Table 2). On one hand this selection criteria was applied for only  $\sim 10\%$  of the sources in Table 1. More importantly, 0140+3253 is the only  $z \geq 3$  radio galaxy from such samples. The other 12  $z \geq 3$  radio galaxies have been found without radio size constraints. This selection can therefore not explain the different LAE fractions at  $z < 3$  and  $z \geq 3$ .

We conclude that no bias is introduced due to radio selection criteria.

Our work is affected by the need to detect strong emission lines since a) this was required in the original sample to measure the redshift b) we need at least Ly $\alpha$  and HeII to be observed to determine whether an object shows Ly $\alpha$  excess. What is clear is that, due to their Ly $\alpha$  excess compared with non-LAEs, we are not likely to have missed low  $z$  LAEs, taking also into account that at low  $z$ , CIV and HeII are in a sensitive part of the spectrographs. There are 26 objects in De Breuck et al (DB00a DB01) at  $2 \leq z < 3$  which could not be classified as LAEs or non LAEs (i.e., Ly $\alpha$ /HeII not available). An extreme, unlikely case of all these objects being LAEs would be required for the fractions of LAEs in the two  $z$  samples to become similar (46% vs. 54%) On the contrary, we would rather expect to have missed non-LAEs in the low  $z$  sample with weak emission lines. This would make the fraction of LAEs in the low  $z$  sample even lower.

Is it possible that the sources with no CIV and HeII are systematically biasing our statistics in the  $z \geq 3$  sample? In the De Breuck et al. (2000) sample, there are 22 objects at  $z \geq 3$ ; 11 of these could not be classified as LAE's or

| $P_{(1400)}/10^{35}$ | Median | Average | $\sigma$ | P   |
|----------------------|--------|---------|----------|-----|
| $2 \lesssim z < 3$   | 1.23   | 1.60    | 1.29     |     |
| $z \geq 3$           | 1.20   | 1.97    | 1.56     |     |
|                      |        |         |          | 18% |

**Table 5.** Comparison between the rest frame radio power at 1400 MHz (in units of  $10^{35}$  erg s $^{-1}$  Hz $^{-1}$ ) for the  $2 \lesssim z < 3$  and  $z \geq 3$  samples. Radio power value taken from DB00a. The median, average and standard deviation values are shown.  $P$  is the probability that the two samples are drawn from different parent populations according to the Kolmogorov-Smirnov test. This tests implies that there is no significant difference in intrinsic radio power between both samples.

non-LAE's. Only 6 of these had HeII outside the observed wavelength range. The remaining 5 sources had too shallow limits on the Ly $\alpha$ /CIV or Ly $\alpha$ /HeII ratio to classify them. Even in the extreme case that these 11 objects were non-LAEs, the fraction of LAEs at  $z \geq 3$  would be 7 out of 22, or 32%, still significantly larger than in the low  $z$  sample.

Is it possible that non-LAEs are systematically missing from samples of HzRGs? In the sample of ultra steep spectrum selected HzRG candidates of De Breuck et al (2001), 13 (35%) sources did not yield a redshift. From these, six did not show any emission, while the other seven had only continuum emission down to the blue end of the spectrograph, but no emission lines. The latter sources have to be at  $z < 2$  (and therefore of no interest in the present work) based on the absence of a continuum discontinuity across Ly $\alpha$ .

The former sources could be at  $z \geq 2$ . The emission lines may be in the observed wavelength range, but too faint to be detected. If they were objects with Ly $\alpha$  in the observed wavelength range, it would have been more likely that they would be non-LAEs, due to their intrinsically fainter Ly $\alpha$  emission. In any case, these sources would add at most six objects to our existing HzRG sample. In the extreme, unlikely case that these were  $z \geq 3$  non-LAEs, the fraction of high  $z$  LAEs would change from 54% to 37%, still significantly larger than in the low  $z$  sample. If these, together with the 11  $z \geq 3$  non-classified objects were  $z \geq 3$  non-LAEs, the fraction would be 25% vs. less than 10% expected in the low  $z$  sample.

We conclude that although the fraction of LAEs may be incompletely determined, both at  $2 \lesssim z < 3$  and at  $z \geq 3$ , the large difference between both fractions is likely to be real and not a consequence of selection effects. An extreme, unlikely situation would be required to change significantly the large difference between the LAE fractions: most non-classified objects at  $2 \lesssim z < 3$  should be LAEs and most non-classified objects at  $z \geq 3$  should be non-LAEs.

In addition, we note that all  $z \geq 3$  LAE's are at  $z > 3.5$ . If we compare the  $z < 3.5$  and  $z > 3.5$  sources, the fraction of LAE's are 4 out of 52 (8%) and 7 out of 9 (78%), respectively. It thus seems impossible to explain such large differences as due to selection effects.

## 7 SUMMARY AND CONCLUSIONS

The behaviour of the Ly $\alpha$ /HeII, Ly $\alpha$ /CIV ratios and the Ly $\alpha$  line luminosity has been investigated in a sample of 48

radio galaxies at  $2 \lesssim z < 3$  and 13 radio galaxies at  $z \geq 3$  for which  $\text{Ly}\alpha/\text{HeII}$  and/or  $\text{Ly}\alpha/\text{CIV}$  measurements are available.

As found by DB00a,  $z \geq 3$  radio galaxies tend to show larger  $\text{Ly}\alpha$  ratios (2.2 and 1.5 times higher for  $\text{Ly}\alpha/\text{HeII}$  and  $\text{Ly}\alpha/\text{CIV}$  respectively) and higher (3 times)  $\text{Ly}\alpha$  luminosities than the low  $z$  sample. The  $\text{Ly}\alpha$  ratios are consistent with or above case B predictions of standard power law photoionization models in at least 54% (7 out of 13) of the  $z \geq 3$  objects. This is the case for only 8% (4 out of 48) of radio galaxies at  $2 \leq z < 3$ . We refer to all these objects with unusually enhanced  $\text{Ly}\alpha$  emission as  $\text{Ly}\alpha$  excess objects or LAEs.

LAEs show  $\text{Ly}\alpha/\text{HeII}$ ,  $\text{Ly}\alpha/\text{CIV}$  and  $\text{Ly}\alpha$  luminosity values which are  $\sim 2$ -3.5 times higher than non-LAEs. They have radio sizes  $\sim 4.6$  times smaller. 36% of LAEs show  $\text{Ly}\alpha/\text{HeII}$  above the standard model predictions. Since in general no absorption has been taken into account, this fraction could be larger.

Several possibilities have been investigated to explain the  $\text{Ly}\alpha$  excess in LAEs: stellar photoionization, shocks, low metallicities, high densities and absorption/resonant scattering effects. All scenarios but the first can be rejected with confidence: we propose that a population of young stars generate the extra supply of soft ionizing photons necessary to produce the observed  $\text{Ly}\alpha$  excess in LAEs. Star forming rates  $\sim 200 M_{\odot} \text{ yr}^{-1}$  are required. The enhanced and intense star formation activity in LAEs could be a consequence of a recent merger event which has triggered both the star formation and the radio/AGN activities. This interpretation is strongly supported by the clear trend for objects with lower optical continuum polarization level to show larger  $\text{Ly}\alpha/\text{HeII}$  ratios. It is further supported by the tentative trend found by other authors for  $z \geq 3$  radio galaxies to show lower UV-rest frame polarization levels, or the dramatic increase on the detection rate at submm wavelengths of  $z > 2.5$  radio galaxies.

The models imply that star formation is occurring in 45% (5 out of 11) of LAEs. Since absorption has not been taken into account, this is a lower limit.

The finding of enhanced  $\text{Ly}\alpha$  emission at tens of kpc from the nuclear region in some objects suggests that star formation can be extended over spatial scales of tens of kpc.

We argue that, although the fraction of LAEs may be incompletely determined, both at  $2 \lesssim z < 3$  and at  $z \geq 3$ , the much larger fraction of LAEs found at  $z \geq 3$  is a genuine redshift evolution and not due to selection effects. Therefore, our study suggests that the radio galaxy phenomenon was more often associated with a massive starburst at  $z > 3$  than at  $z < 3$ . In other words, powerful radio galaxies (and, according to the unification model, powerful radio quasars), appear in more actively star forming galaxies at  $z > 3$  than at  $z < 3$ .

Enhanced  $\text{Ly}\alpha$  ratios in the extended gas of some  $z < 3$  radio galaxies suggest that star formation is also present in these objects, although at lower levels. Star formation could also be responsible for the  $\text{Ly}\alpha$  emission from regions out of the reach of the quasar continuum and the radio structures detected in some high redshift radio galaxies.

We propose to use the  $\text{Ly}\alpha$  ratios (specially  $\text{Ly}\alpha/\text{HeII}$ ) of high redshift ( $z \gtrsim 2$ ) radio galaxies and the extended gas in radio loud and radio quiet quasars to investigate the possible signature of star formation.

## ACKNOWLEDGMENTS

We thank the anonymous referee for very useful comments which helped to improve this paper substantially and Enrique Pérez for useful comments on the manuscript. We thank Mark Allen for providing predictions of emission line ratios for the most recent shock models, which include high velocities of up to  $1000 \text{ km s}^{-1}$ . The work of MVM has been supported by the Spanish Ministerio de Educación y Ciencia and the Junta de Andalucía through the grants AYA2004-02703 and TIC-114 respectively. AH acknowledges support in the form of a UNAM postdoctoral fellowship.

## REFERENCES

- Archibald E., Dunlop J., Hughes D., Rawlings S., Eales S., Ivison R., 2001, MNRAS, 323, 417
- Best P., Röttgering H., Longair M., 2000, MNRAS, 311, 23
- Bicknell G., Sutherland R., van Breugel W., Dopita M., Dey A., Miley G., 2000, ApJ, 540, 678
- Binette L., Dopita M. & Tuohy I., 1985, ApJ, 297, 476
- Binette L., Wang J., Villar-Martín M., Martín P., Magris C., 1993, ApJ, 414, 535
- Chini R., Krügel E., 1994, A&A, 288, L33
- De Breuck C., van Breugel W., Miniti D., Miley G., Röttgering H., Stanford S., Carilli C., 1999, A&A, 352, L51
- De Breuck C., Röttgering H., Miley G., van Breugel W., Best P., 2000a, A&A, 362, 519 (DB00a)
- De Breuck C., van Breugel W., Röttgering H., Miley G., 2000b, A&AS, 143, 303
- De Breuck et al., 2001, AJ, 121, 1241 (DB01)
- De Robertis M. & Osterbrock D., 1984, ApJ, 286, 171
- Dey A., van Breugel W., Vacca W., Antonucci R., 1997, ApJ, 490, 698
- Dopita M., Sutherland R., 1996, ApJSS, 102, 161
- Dunlop J., Hughes D., Rawlings S., Eales S., Ward M., 1994, Nature, 370, 347
- Ferruit P., Binette L., Sutherland R., Pecontal E., 1997, A&A, 322, 73
- Fosbury R. et al., 2003, ApJ, 596, 797
- Hansen M., Oh S., 2006, MNRAS, 367, 979
- Heckman T., Lehnert M., Miley G., van Breugel W., 1991a, ApJ, 381, 373
- Heckman T., Miley G., Lehnert M., van Breugel W., 1991b, ApJ, 370, 78
- Humphrey A., 2005, PhD Thesis, Univ. of Hertfordshire
- Humphrey A., Villar-Martín M., Fosbury R. Vernet J., di Serego Alighieri S., 2006, MNRAS, 369, 1103
- Jannuzi B., Elston R., Schmidt G. Smith P., Stockman H., 1995, ApJ, 454, 111
- Larkin et al., 2000, ApJ, 533, 61
- Leitherer C. et al., 1999, ApJS, 123, 3
- Martín-Mirones J.M., Martínez-González E., González-Serrano I., Sanz J.L., 1995, ApJ, 440, 191
- Maxfield L., Spinrad H., Stern D., Dey A., Dickinson M., 2002, AJ, 123, 2321
- McCarthy P., 1991, AJ, 102, 518
- McCarthy P., van Breugel W., Kapahi V., Subrahmanya C., 1991, AJ, 102, 522
- McCarthy P., 1993, ARA&A, 31, 639

- Overzier R., Röttgering H., Kurk J., De Breuck C., 2001, *A&A*, 367, L50
- Reuland M., van Breugel W., Röttgering H., de Vries W., Standford S., Dey A., Lacy M., Bland-Hawthorn J., Dopita M., Miley G., 2003, *ApJ*, 592, 755
- Reuland M., Röttgering H., van Bruegel W., De Breuck C., 2004, *MNRAS*, 353, 377
- Robinson A., Binette L., Fosbury R., Tadhunter C., 1987, *MNRAS*, 227, 97
- Scheuer P., 1995, *MNRAS*, 277, 331
- Steidel C., Pettini M., Adelberger K., 2001, *ApJ*, 546, 665
- Stevens et al., 2003, *Nature*, 425, 264
- Tadhunter C., Robinson T., González-Delgado R., Wills K., Morganti R., 2005, *MNRAS*, 356, 480
- Van Ojik R., Röttgering H., Carilli C., Miley G., Bremer M., Macchetto F., 1996, *A&A*, 313, 25
- Van Ojik R., Röttgering H., Miley G., Hunstead R., 1997, *A&A*, 317, 358
- Vernet J., Fosbury R., Villar-Martín M., Cohen, M. H., Cimatti, A., di Serego Alighieri, S., Goodrich, R. W., 2001, *A&A*, 366, 7
- Vila Costas M., Edmunds M., 1993, *MNRAS*, 265, 199
- Villar-Martín M., Binette L., Fosbury R., 1996, *A&A*, 312, 751
- Villar-Martín M., Fosbury R., Binette L., Tadhunter C., Rocca-Volmerange, 1999, *A&A*, 351, 47
- Villar-Martín M., Tadhunter C., Clark N., 1997, *A&A*, 1997, 323, 21
- Villar-Martín M., Vernet J., di Serego Alighieri S. et al., 2003, *MNRAS*, 346, 273
- Villar-Martín M., Cerviño M. & González Delgado R., 2004, *MNRAS*, 355, 1132
- Villar-Martín M., Tadhunter C., Morganti R., Holt J., 2005, *MNRAS Letters*, 359, 5
- Willott C., Rawlings S., Blundell K., Lacy M., 1999, *MNRAS*, 309, 1017
- Wilman R., Jarvis M., Röttgering, Binette L., 2004, *MNRAS*, 1109
- Zirm et al. 2005, *ApJ*, 630, 68